Metallophysics and Advanced Technologies
Металофіз. новітні технол.
Metallofiz. Noveishie Tekhnol.
2022, vol. 44, No. 10, pp. 1275–1292
https://doi.org/10.15407/mfint.44.10.1275
Reprints available directly from the publisher

PACS numbers: 07.10.-h, 68.35.Fx, 68.35.Rh, 68.55.Ln, 81.40.-z

Thermal and Ion Treatment Effect on Nanoscale Thin Films Scratch Resistance

V. Yanchuk[*], I. Kruhlov[*], V. Zakiev[*,**], A. Lozova[*], B. Trembach[***], A. Orlov[*], and S. Voloshko[*]

[*]*National Technical University of Ukraine 'Igor Sikorsky Kyiv Polytechnic Institute', 37 Peremohy Ave., UA-03056 Kyiv, Ukraine*
[**]*National Aviation University, 1 Lyubomyr Huzar Ave., UA-03058 Kyiv, Ukraine*
[***]*Private Joint Stock Company 'Novokramatorsky Mashinostroitelny Zavod', 5 Oleksa Tikhoy Str., UA-84305 Kramatorsk, Ukraine*

In this study, a microtribological characteristics of Ni(25 nm)/Cu(25 nm)/Cr(25 nm) three-layer thin films fabricated using DC magnetron sputtering are explored using progressive scratch test. Four various types of thin films are examined and compared: as-deposited film, film after low-energy Ar^+ ion irradiation, film annealed at 450°C for 15 minutes in vacuum, and film after ion irradiation followed by vacuum annealing. Scratch tests are supplemented by structural (XRD) and chemical (AES) experimental studies. As figured out, the sample after ion irradiation followed by annealing demonstrated the best microtribological and wear resistance characteristics among all studied films. The highest scratch resistance, smooth scratch shape, the lowest value of peak tangential force as well as the absence of side cracks and film delamination are revealed for the sample after irradiation followed by annealing. The likely reasons of this behaviour are discussed.

Key words: thermal and ion treatment, thin films, scratch resistance, microtribological resistance, scratch test.

Corresponding author: V. Yanchuk
E-mail: yan4uk.v@gmail.com

Citation: V. Yanchuk, I. Kruhlov, V. Zakiev, A. Lozova, B. Trembach, A. Orlov, and S. Voloshko, Thermal and Ion Treatment Effect on Nanoscale Thin Films Scratch Resistance, *Metallofiz. Noveishie Tekhnol.*, **44**, No. 10: 1275–1292 (2022). DOI: 10.15407/mfint.44.10.1275

У даній роботі за допомогою методи склерометрії досліджено мікротрибологічні характеристики тришарових нанорозмірних композицій Ni(25 нм)/Cu(25 нм)/Cr(25 нм), одержаних методою магнетронного осадження. Досліджено чотири різні типи нанорозмірних композицій: після осадження, після опромінення низькоенергетичними йонами Ar^+, після відпалу у вакуумі за температури 450°C впродовж 15 хвилин і після йонного опромінення з наступним вакуумним відпалом. Результати мікротрибологічних випробувань доповнено даними структурних (РСФА) та хемічних (ОЕС) досліджень. Встановлено, що найкращі мікротрибологічні та зносостійкі характеристики серед усіх досліджуваних зразків виявлено для випадку йонного опромінення з наступним відпалом. Для цього зразка зафіксовано найвищу зносостійкість, чітку форму подряпини, найменше значення максимальної танґенційної сили, а також відсутність бічних тріщин і розшарування плівки. Обговорюються ймовірні причини такого ефекту.

Ключові слова: термічне та йонне оброблення, тонкоплівкові композиції, зносостійкість, мікротрибологічна стійкість, склерометрія.

(Received July 28, 2022; in final version, August 11, 2022)

1. INTRODUCTION

Thin films are widely used as functional, reinforcing, reflective, conductive, and dielectric materials in the manufacture of printed circuit boards, integrated circuit elements in microelectronics, light filters, optoelectronic elements, in novel lithographic processes, as well as for the development of new generation contacts for solar cells based on silicon, graphene, perovskite and their combination.

In particular, the modern microelectronics industry is developing based on nanoscale devices. Of the most important components of such systems, there are heterogeneous materials based on complex nanoscale multilayer structures [1].

It is acknowledged that the reliability of electronic devices significantly depends on the strength of interatomic interaction at the interfacial boundaries. A measure of this interaction is the adhesive strength, which plays an important role in multilayer thin-film systems, in particular, at the film/film and film/substrate interfaces [2]. Adhesion is a key factor determining the durability of thin-film devices, for example, in microelectronic integrated circuits, affecting the probability of film delamination. In solar energy, the efficiency of photoconversion in CIGS modules also largely depends on the adhesion of the metal back contact, provided that its high conductivity is maintained [3]. In this regard, the measurement of the adhesion force has become one of the most important tasks in the development of various technological processes of microelectronics and photovoltaics [4–6].

An effective way to increase adhesion in the case of thin-film coat-

ings is the intentional formation of transition layers by the diffusion of one metal into another, the formation of intermetallics at their interfaces, the interaction of metal with oxygen from the substrate [7].

Thin layers of various metals with high oxygen affinity are usually applied to the substrate to enhance the adhesive strength [8]. However, it should be considered that the adhesion depends not only on the oxygen affinity of the metal, but also on other factors such as residual oxygen pressure in the deposition chamber, film structure *etc*. The mechanism of intermediate layer formation in this case is mediated by the oxygen diffusion from various sources (spray chamber, metal film, oxides) to the metal/oxide interface [7]. Thus, a contradiction arises: on the one hand, the physicochemical interaction of metal films with each other and the substrate is desirable, and on the other hand, such interaction disrupts the thermal stability of metal contacts and their conductivity due to oxygen diffusion during oxide decomposition on thermal exposure. As a result, the functionality of such products can be severely affected not only by various mechanical problems, such as delamination and buckling, but also by changes in phase and chemical composition. This problem is even more complicated in the case of multilayer nanoscale coatings.

Ion bombardment is considered to be one of the effective tools for adhesion enhancement. One of the first works in this direction [9] showed that the argon bombardment with a dose of 10^{15}–10^{16} ions/cm^2 and an energy of 80–120 keV of aluminium films with a thickness of 400–500 Å allows to increase the peeling strength between the film and glass substrate by about two orders of magnitude. According to the authors, this effect causes the formation of an intermediate structure at the glass-aluminium interface, which increases the strength of adhesion. Advantages of ion implantation under high-energy irradiation have been widely reported in the literature [10]. However, the range of low beam energies (< 3 keV) is of high interest for modern nanotechnologies to restrict the radiation damage of the structure. That is due to the fact that the implantation of inert gas ions and the degradation of the optical properties of nanosize coatings occur at energies up to 5 keV [11].

Low-energy ion irradiation of substrates has proven itself well in terms of increasing adhesion [12], including the creation of thin-film photoconverters for solar technology [3]. Today, the methods of ion assistance in the deposition of thin films on different substrates have become especially widespread. It has been reported that the presence of the ionic component directly during sputtering leads to the formation of compressive stresses [13], reduction in grain size and suppression of the columnar structure [14]. On the other hand, excessive stresses can lead to the adhesion degradation and, as a consequence, to the film cracking and peeling. The possible various effects of ion bombardment on the adhesion of different metals related to the degree of affinity of

the irradiated metal to oxygen should be taken into account. Ion bombardment at low energies can cause both oxidation of the metal and reduction of already formed oxides [15].

This can provide additional opportunities to improve the properties of the conductive layer after the deposition of the layered structures [16] and before the subsequent technological operations associated with thermal exposure.

Thus, the study of the effect of low-energy ion radiation on the adhesion of thin metal films, the choice of energy and duration of processing, substrate temperature and other parameters, is an important technological problem.

As for experimental techniques for quantifying the adhesion of thin films, quite a lot of them have appeared in recent decades. The most effective methods include the following: four-point bending (4PB), bending test, microcantilever tests, spontaneous bulging, nanoindentation, and scratching [17–19].

It has been earlier reported the results of the pin-on-disk microtribological test using the Rockwell indenter which allowed to estimate the wear resistance and adhesion strength of the nanoscale Cr(25 nm)/Cu(25 nm)/Ni(25 nm) system [20].

However, one of the most informative analytical methods for the characterization of adhesive properties remains the scratch test [21–23]. It was one of the first techniques to be widely used to assess the strength of materials [24], although for some time local indentation almost completely replaced scratch testing in engineering practice. However, in recent years, scratch testing has returned not only to scientific laboratories, but also has become an effective method of quality control in the high-tech industry [23].

During scratch test, indenter is pressed into the material surface under the action of normally applied load with simultaneous sample movement fixed on a motorized stage [25]. Depth, width, and shape of generated scratch on the sample surface depend on the material scratch resistance and its resistance to destruction. Moreover, modern scratch testers are equipped with sensitive displacement sensors, allowing to register lateral or normal indenter displacement during the test providing new opportunities for evaluation materials behaviour under load, fracture resistance and mechanical properties. Depending on the combination of different factors, it is possible to study various mechanisms of scratch formation (plastic deformation, cutting, dispersing, brittle chipping, as well as their combinations) [26].

Scratch tests can be divided into static and progressive depending on load application law. During static tests, a scratch is generated on the sample surface by application of constant indenter load. This type of test is generally used to evaluate the tribological properties of different materials or to calculate hardness by scratching. Quantitative val-

ues of hardness are determined either by the width of the scratch (scratch hardness) or by the magnitude of the tangential force required to form a scratch (plugging hardness) [27]. This approach has been widely applied for studying the materials with a porous [28], multiphase or composite structure [29, 30].

The progressive mode assumes that during scratching the normal load on the indenter gradually increases from zero to the predetermined value over time. This test mode is widely used in studies of the adhesive properties of various coatings [10, 31, 32] and submicron-thick films obtained by magnetron deposition [33]. The mechanism of coating destruction depends on the instrument features and settings (loading speed, scratching speed, indenter type and shape), properties of the substrate (hardness and elasticity modulus) and the coating itself (thickness, hardness, elasticity modulus, residual stresses, surface roughness *etc*.). [34]. During progressive scratching, local defects are formed in the studied coatings, so one of the most important characteristics is the critical load L_c that initiates coating failure [35]. Moment of coating failure is determined from friction force analysis or microscopic examination of formed scratch.

The objective of present study is to evaluate the scratch resistance and adhesive strength of nanoscale Ni/Cu/Cr system after ion and/or heat treatment using the progressive scratch test.

2. METHODS AND OBJECTS

Ni(25 nm)/Cu(25 nm)/Cr(25 nm) thin films were fabricated by magnetron deposition onto single crystal Si (001) substrates at room temperature from high-purity targets of Ni (99.995 at.%), Cu (99.99 at.%), Cr (99.95 at.%). Before deposition, the substrate was subjected to standard ultrasonic cleaning. Additional oxidation of the silicon single crystal surface was not used, but the already formed layer of natural SiO_2 oxide of several nanometres thickness was not removed. Additional oxidation could help to improve the mechanical characteristics of the structure due to the formation of an intermediate layer of Cr_xO_y oxide [36].

Low-energy Ar^+ ion bombardment of films surfaces was carried out using an OMI-0010 accelerator with an energy of 800 eV with a duration of 20 minutes and a fluence of $5 \cdot 10^{16}$ ion/cm^2, which was precalibrated using the standard Faraday cup. Because low beam energies were applied, no noticeable heating of the samples was observed when irradiated, heating was controlled by a *K*-type thermocouple mounted on the film surface.

Heat treatment of the samples was performed in a vacuum of 10^{-3} Pa at a temperature of 450°C for 15 minutes at a heating rate of 2°C/s. The combined mode provided ion treatment with an energy of 800 eV

lasting 20 minutes and fluence of $5 \cdot 10^{16}$ ion/cm^2 followed by heat treatment in a vacuum of 10^{-3} Pa at 450°C for 15 minutes at a heating rate of 2°C/s.

To study the scratch resistance and adhesion strength of Ni/Cu/Cr thin films with substrate, a series of scratch tests were performed using the multifunctional indentation tester 'Micron-gamma' [37]. The indentation tester is equipped with a built-in optical microscope, which allow precisely select surface area for investigation and get images of formed scratches immediately after test. This allows to characterize the mechanisms of surface destruction, as the tested specimen with the formed defects remains static on the instrument motorized stage and does not require any movement for further analysis.

Thin films in the initial state, as well as after ion, thermal and combined effects were studied by the progressive scratch testing. Scratching was performed with a Berkovich diamond indenter, with a gradual increase of indenter load from 0 to 100 mN and its subsequent gradual decrease from 100 to 0 mN, while the loading and unloading rates were 10 mN/s. Proposed loading law allows to determine not only the moment of coating failure, but also the load at which the indenter will return back on the coating surface during unloading, providing additional information about coating resistance to fracture. The use of a sharp indenter localizes the maximum stresses closer to the surface and minimizes the substrate deformation [38].

Surface scratching was realized by the automated movement of the motorized sample stage of the instrument in two-dimensional plane. The length of each scratch was 600 μm. With the help of a precision system of indenter displacements measurements, the values of the tangential (friction) force were registered. Analysis of the tribograms (dependence of the friction force along scratch distance) allowed us to estimate the moment of film failure and to determine the interfaces between different layers of layered stacks. It should be noted that the ability to register the tangential or friction force during the scratch measurement allows to study the surface properties of thin-film and nanoscale materials, as well as practical adhesion between film and substrate [39].

Structural properties and phase composition of thin films after deposition and post-annealing were studied by x-ray diffraction (XRD), using synchrotron radiation and grazing-incidence wide-angle x-ray scattering (GIWAXS) technique at BL44B2 RIKEN SPring-8 Materials Science Beamline. The Debye–Scherrer camera of 286.5 mm radius was equipped with an image plate 400×200 mm detector. The grazing angle between the beam and the sample surface was 0.5°, while the x-ray wavelength was adjusted to 0.8 Å. Vertical and horizontal beam sizes were 0.01 mm and 3.0 mm, respectively. Averaged crystallites size (or coherence length) of film layers was evaluated using Scherrer's formula by determining the full width at half maximum (FWHM) of

the diffraction lines.

Chemical composition of as-received and post-annealed film samples was studied by Auger electron spectroscopy (AES) measurements at Jamp-9500F (Jeol) device. AES chemical depth profiling was carried out by etching the surface of the films with 1 keV Ar^+ ions at a 45° incidence angle to the sample surface. Spectra were obtained at the primary electron beam energy of 10 keV and a current of 30 nA with a 0.6% resolution.

3. EXPERIMENTAL RESULTS

Scratch test showed a different nature of the Ni/Cu/Cr film failure for samples in the initial state, after ion treatment, after annealing and a combination of ion and heat treatment, despite the similar chip formation mechanisms.

The analysis of the registered tribograms and surface images showed a significant influence of different processing types on film layers adhesion force. Tribogram for the film in the initial state shows a gradual destruction of each layer, accompanied by a change in the angle of tangential force. Critical loads (L_c) at which the destruction of each layer occurs for the initial state and different treatment modes are shown in Table 1.

Scratch test results for as-deposited specimen are shown in Fig. 1, *a*. The lower part of the figure represents a tribogram, that characterizes the resistance of the material to the indenter movement along the scanning path during scratching at a constant speed with increasing indenter load from 0 to 100 mN and its decreasing from 100 mN to 0. Top of the figure shows optical microscopy image of the corresponding scratch on the sample surface. The initial stage of scratching is characterized by a gradual increase in friction force during loading, as well as the absence of microcracks and wear products. When the load reaches 19 mN, the angle of the tribogram changes, which indicates the destruction of the surface layer (Ni). As the load increases, the wear products and cracks appear along the scratching path. The destruction of the intermediate layer (Cu) occurs at load of 62 mN, and the Cr layer destruction takes place at load of 96 mN, which is accompanied by changes in the angle of tangential force. It should also be noted that the load at which the indenter returns to the surface of each layer during unloading is slightly lower than the load required for the destruction of the film layers, and it is 87 mN, 54 mN and 8 mN for each layer respectively. This trend (fracture load is always higher than the load at which the indenter returns on the surface of each layer during unloading) is observed in all samples and can characterize the resistance of coatings to scratch fracture. Lee and Liu reported [40] that nanoindentation causes atomic reorganization and leads to the formation of areas of high-stress plastic defor-

TABLE 1. Critical loads for the initial state and different treatment modes.

Specimen		Loading			Unloading		
	Thickness, nm	$L_{c\,Ni}$, mN	$L_{c\,Cu}$, mN	$L_{c\,Cr}$, mN	$L_{c\,Cr}$, mN	$L_{c\,Cu}$, mN	$L_{c\,Ni}$, mN
As-deposited	75 nm	19	62	96	87	54	8
Annealed	75 nm	14	60	94	70	50	6
Ion irradiated	66.8 nm	–	74	90	60	54	–
Irradiated and annealed	66.8 nm	–	76	–	–	72	–

mation and even to the selective segregation of elements around the indenter imprint. It is likely that during continuous scratching, stresses in material affect the value of the critical load at which the indenter return on each layer surface compared to the fracture load.

The scratch test results for the sample after ion irradiation with an energy of 800 eV for 20 minutes (Fig. 1, *b*) has showed that despite similar stages of deformation and destruction to those observed for the original sample, there are some differences. The lateral microcracks appear in the load region of 60 mN that corresponds to the transition to the last layer of the stack. It should also be noted that after the complete destruction of all layers, there is a fragile destruction of the coating and its delamination along the edges of the scratch, even during further unloading to 70 mN, accompanied by nonmonotonic and uneven changes of the tangential force. It can be assumed that there is a significant excess of fracture stress over the critical fracture toughness in this region, resulting in the formation of chips and cracks [41]. At the same time, further unloading of the indenter at the range of 50–0 mN is characterized by the complete absence of cracks and chips and a smooth shape of the scratch similar to the initial stage of scratching.

Figure 1, *c* shows the results of scratch test of annealed sample, which demonstrates a completely different nature of deformation and fracture compared to the as-deposited film. It is not possible to identify the areas of the film delimitation for this sample. During scratching there is a monotonic increase of tangential force to a critical fracture load, that corresponds to the destruction of the entire coating. The critical load of 74 mN corresponds to fracture of first two coating layers. During the unloading of the indenter the process of the coating fracture is completed at load value of 54 mN. It should also be noted that at a load of 90 mN, fragile destruction of the all film layers is observed along the scratching path. It is accompanied by a higher level of tangential force for the annealed sample as the stress state of the system increases. Large amount of wear products around the scratch and

delamination of the film are seen, which means relatively low resistance to fracture and low adhesion. It is likely that the heat treatment causes diffusion blurring of the interfaces between the metal layers and impairs the tribological and adhesive properties of the film compared to the initial state.

Figure 1, *d* shows the results of scratch test for the sample after combined treatment. It should be noted that applied load does not cause failure of all the film layers and its delamination from substrate. Fracture of first two film layers is observed at load 76 mN during loading and finished at 72 mN during unloading phase. The difference between these values is the smallest among all studied samples. Experimental result shows the highest scratch resistance of the irradiated and annealed film compared to its condition after the heat treatment only. Moreover, unlike previous cases, the scratch has a clear shape with a minimal width, there are no signs of brittle destruction and delamination of the film, as well as small amount of wear products. In this case, the lowest peak value of the tangential force is registered, which is more likely due to the deformation of the film, rather than its separation from the substrate.

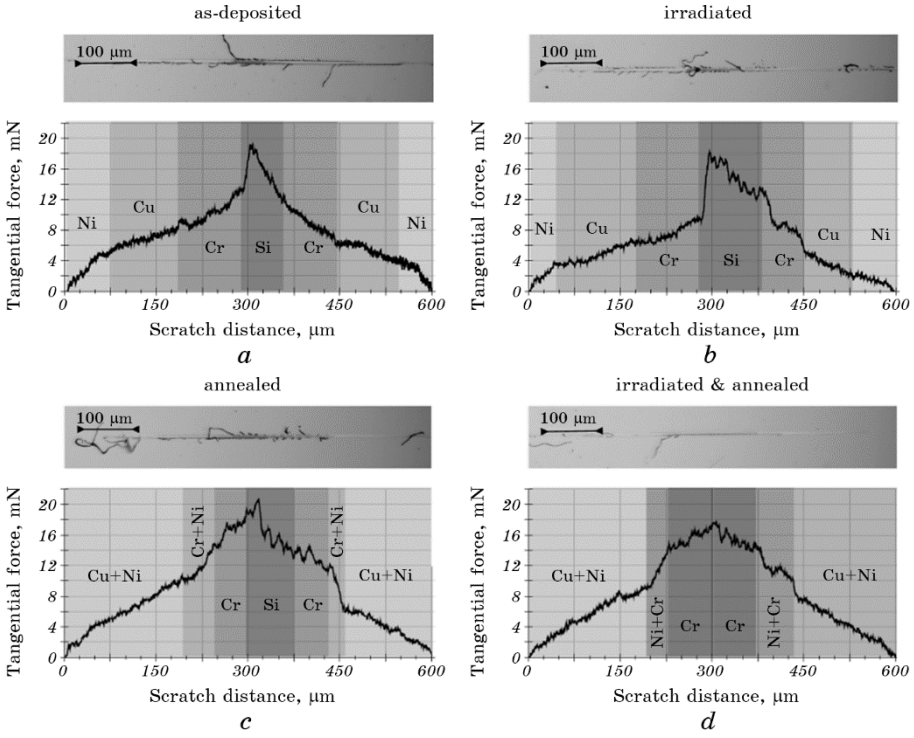

Fig. 1. Tribograms of the as-deposited (*a*), ion irradiated (*b*), annealed (*c*) and irradiated and annealed thin-film samples (*d*).

It is worth noting that along the entire length of the scratch, no lateral cracks and no coating destruction were detected. In addition, the scratch itself is smooth and without fractures and wear products. All the above indicate that complex processing is useful to enhance the microtribological and adhesive properties of the film.

A rough estimation of the adhesion strength ratio after treatment to initial sample is performed using the method described elsewhere [21], taking into account the value of critical load, scratch track radius and coating thickness. It shows that after annealing the adhesion increases in 1.5 times compared to the initial state, after ionic treatment in 1.4 times, while after complex treatment in 5.8 times.

4. DISCUSSION

To understand the reasons of the established difference in tribological properties, an analysis of the structural phase transitions of all samples has been done using the XRD technique. Figure 2 shows synchrotron XRD scans of the thin-film samples after deposition and after different types of processing. The change of average crystallite size (Fig. 2, *b*) and lattice parameters (Fig. 2, *c*) as a function of treatment conditions are also presented.

For the initial state, a set of diffraction peaks characteristic to the f.c.c. Ni, f.c.c. Cu, and b.c.c. Cr phases is observed. The lattice parameters of the Ni, Cu and Cr phases, calculated based on the XRD data, are presented in Fig. 2, *b*. In the initial state, the lattice constants of these phases are 0.351 nm, 0.359 nm, and 0.289 nm, respectively. Further ion treatment does not change the initial phase composition, the appearance of new peaks from oxides or other compounds is not observed, and the lattice parameters of all phases remain unchanged. The decrease in the integral intensity of the Ni peak is associated with its sputtering during ion irradiation stage, and in the case of annealing also with the diffusion of Cu to the outer surface. The shift of the angular position of the Cu (111) peak towards the position of the Ni (111) peak after annealing indicates the formation of a Cu-based solid solution. However, the decrease in the Cu lattice parameter is insignificant and indicates that the Ni concentration in this solid solution does not exceed 5%. The angular position of the Ni peak remains almost unchanged, so there is no noticeable change in the parameter of its crystal lattice. After annealing with additional ion pre-treatment, no significant changes were recorded compared to the case of annealing only.

The Ni crystallite size is almost twice that of Cu in the initial state, which is one of the factors that explains the accelerated diffusion of Ni into Cu in contrast to the bulk material. After ion treatment, the crystallite size of Ni decreases to ~ 6.7 nm, and after annealing at 450°C it increases to ~ 11 nm compared to the initial state (~ 9.5 nm). After the

combined treatment, the most significant decrease in Ni crystallite size down to 5 nm is observed. Decrease in the grain size, respectively, reduces the surface roughness and increases the adhesive strength, which is in a good agreement to the experimental data [6] and the base model [42].

The AES layer-by-layer elemental composition of as-received sample is shown in Fig. 3, *a*. Clear interfaces between the layers indicate that no diffusion intermixing is taking place after DC magnetron sputtering. Accordingly, the tribograms clearly indicates separation between

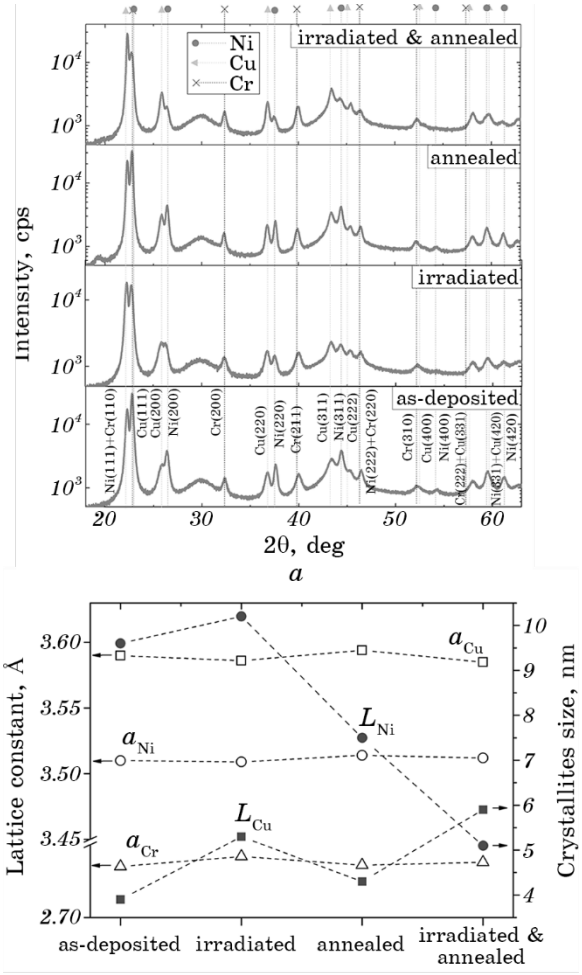

Fig. 2. XRD scans (*a*) of thin films after deposition and different treatments; the change of crystallite size and lattice constant (*b*) for all samples is given as well.

individual layers and the moment when the indenter reaches the substrate with a characteristic burst of tangential force.

Heat treatment in vacuum promotes the activation of diffusion processes. Mutual diffusion of Ni and Cu is observed on the Auger profiles (Fig. 3, *c*). Cu atoms diffuse towards the film outer surface, their concentration in the Ni subsurface area reaches 15–18 at.%. The increased oxygen content up to 30 at.% in this layer indicates the possible Cu oxidation. The presence of surface contaminants or oxide layers can significantly affect the adhesive strength [43].

Ni atoms also diffuse into the Cu layer in the amount of about 10 at.%, while at the interface with Cr its presence reaches 20 at.%. After annealing, the sputtering time of the Cr layer increases markedly during the analysis, which might be associated with the formation of dispersed carbide phases near the substrate, although their presence has not been recorded by XRD. The amount of carbon in the Cr increases to approximately 10 at.% throughout the layer, while for the as-deposited sample it does not exceed 2–3 at.%. However, the amount of C increases at least in 3 times compared to the initial state, according to the es-

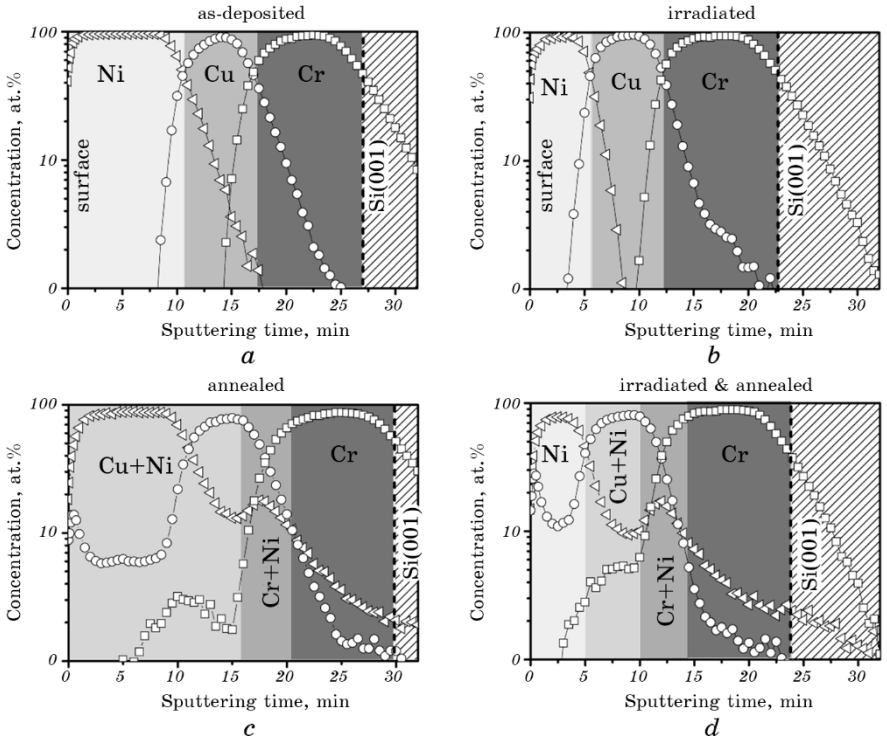

Fig. 3. Auger layer-by-layer elemental distribution of the as-deposited (*a*), ion irradiated (*b*), annealed (*c*) and irradiated and annealed thin-film samples (*d*).

timation of the integrated area occupied by C in the Cr layer. It should be noted that Cr is a carbide-forming element (enthalpies of formation of carbides $Cr_{23}C_6$, Cr_7C_3, Cr_3C_2 are -290.0 ± 27.6 kJ/mol, -149.2 ± 8.5 kJ/mol, -81.1 ± 2.9 kJ/mol, respectively) [44]. Additionally, reduction processes at the internal interfaces that could take place during vacuum annealing, could also adversely affect the adhesion strength of the film to the substrate. The region, corresponding to the Ni and Cu intermixing, is also seen at the tribograms, as well as the Cr layer and Cr/Si interface are also distinguished. The transition layer of different tribological properties is clearly seen between Cu and Cr. It contains Ni atoms and according to the binary phase diagram, eutectic mixture of Ni with Cr is possible. Existence of such Ni–Cr eutectic phase compound can be also indirectly judged by the change in the inclination angle of tangential force on the corresponding tribogram.

The diffusion coefficients of Ni and Cu were estimated based on the AES concentration profiles using the centre-gradient approach proposed by Hall and Morabito [45]. The method is based on the assumption that the lattice diffusion is the dominating mechanism at the interfaces between metal layers, while the grain boundary contribution can be neglected. The degree of initial diffusion, *i.e.*, before annealing, has also been taken into account. In present case, the concentration profiles of the components (given in logarithmic coordinates) after annealing (Fig. 3, *c*) and for the initial state (Fig. 3, *a*) were compared. The estimated lattice diffusivities of Ni in Cu and Cu in Ni after vacuum annealing at 450°C for 15 minutes are summarized in Table 2. The literature data on the Ni and Cu diffusion coefficients in thin-film systems is given as well as for a reference. According to the results obtained, both diffusion coefficients are in the range 10^{-17}–10^{-18} cm^2/s, but Cu in Ni diffusivity coefficient is higher than the Ni in Cu one. In order of magnitude, our data are in good agreement with the data reported by Lian *et al.* [46], where the Hall–Morabito method was also applied. Moreover, the authors proved that this method has good accuracy for the case of thin films and the influence of sputtering artefacts can be neglected.

The Auger depth profiling characterizes the average distribution in chemical composition through the film thickness, *i.e.*, provides integrated information on grain boundary and bulk diffusion mechanisms. XRD data characterize bulk diffusion, when phase transformations take place with the gradual formation of a homogeneous solid solution. Thus, the observed intermixing between Ni and Cu, which is not accompanied by significant changes in the parameters of the crystal lattice according to XRD data, indicates a predominantly grain boundary diffusion mechanism. This mechanism does not enhance the interatomic interaction between the film layers and does not improve adhesion.

In addition, the reduction of interfacial oxide layers, which may form during magnetron sputtering, could take place during vacuum

TABLE 2. Lattice diffusion coefficients of Ni in Cu and Cu in Ni.

	Diffusion couple	D, cm^2/s	Treatment	Reference
Cu in Ni	Ni(25 nm)/Cu(25 nm)	$5.8 \cdot 10^{-17}$	450°C	Present study
	Ni(25 nm)/Cu(25 nm)	$5.3 \cdot 10^{-17}$	Pre-irradiation, 450°C	Present study
	Ni(100 nm)/Cu(100 nm)	$3.8 \cdot 10^{-17}$	400°C	[46]
Ni in Cu	Ni(25 nm)/Cu(25 nm)	$9.2 \cdot 10^{-18}$	450°C	Present study
	Ni(25 nm)/Cu(25 nm)	$2.1 \cdot 10^{-17}$	Pre-irradiation, 450°C	Present study
	Ni(100 nm)/Cu(100 nm)	$6.1 \cdot 10^{-18}$	400°C	[46]

annealing [47]. The reduction of such oxides or suboxides adversely affects adhesion. And the formation of chromium silicide, which enhances an adhesion, at this temperature does not occur [40]. As a result, the tribological and adhesive properties of the film after annealing compared to the initial state deteriorate, which is manifested in a decreased critical load. Thus, the simultaneous influence of such factors as enlargement of crystallite size, increase of surface roughness, saturation of the Cr layer with carbon, reduction of oxides at the interfaces adversely affects the adhesive strength of thin films.

After ion irradiation at the energy of 800 eV for 20 minutes (Fig. 3, *b*), the Ni layer is sputtered with a corresponding decrease in its thickness from 25 to 16 nm. However, irradiation does not induce a diffusion interaction of components and there are no changes in the phase composition. Ion treatment with the mode used helps to reduce the amount of O and C remained in the film after deposition stage, as well as to increase the concentration of Cu from 90% to almost 100%. The development of reduction processes at the internal interfaces is associated with the long-range effects induced by low-energy ions, which has been discussed in detail elsewhere [15]. Optimal ion treatment mode (energy of 800 eV and fluence of $5.6 \cdot 10^{16}$ ion/cm^2) caused a simultaneous passivation of all film layers with decreased presence of oxygen and carbon impurities. Since reduction processes yield first of all at the Cr/Si interface, it brings light on the change in destruction behaviour in this area. Reducing the size of the crystallite size of the Ni layer to ~ 8 nm compared to the initial state (~ 13 nm) should increase the resistance to failure, but the thickness of the Ni layer decreases to 16 nm, which likely compensate the effect. Ion irradiation increases the Ar content due to the ion implantation, which is a well-known effect [48]. However, ion irradiation also leads to a significant increase in the number of point structural defects, which is likely to be the cause of the experimentally observed degradation of adhesion and wear

resistance of the irradiated sample. It should be emphasized that there is rather contradictory information on the effect of ion irradiation on surface strength properties in the literature. Positive and negative effects of irradiation on strength characteristics have been reported, usually associated with ion-induced residual stress modification, surface atom packing factor, and surface lattice density regulated by the concentration of implanted ions [49, 50].

However, the combination of ion and thermal treatments improves the microtribological characteristics of Ni(25 nm)/Cu(25 nm)/Cr(25 nm) three-layer stack, which is in a good agreement to the previously observed effect reported for Cr(25 nm)/Cu(25 nm))/Ni(25 nm) films [20]. The improvement of mechanical properties is observed compared both to the annealed sample and as-deposited film. Ion treatment before annealing does not affect noticeably the elemental distribution of the main components compared with thermal annealing (Fig. 3, *d*).

Grain-boundary diffusion of Cu atoms intensifies, their number increases both directly on the outer surface (up to 25 at.%) and in the near-surface region of the Ni layer. The diffusion of Ni atoms into the Cu layer is slightly accelerated in the region near their interface, which strengthens the interatomic bond between Ni and Cu, but in the Cu layer, on the contrary, it slows down. The amount of Ni also decreases at the Cu/Cr interface, which is positive for the adhesion as the amount of the Ni + Cr eutectic mixture decreases. The reduction in the amount of carbon in the Cr layer compared to heat treatment (about 1.3 times) is another factor that positively affects adhesion strength.

The estimation of the diffusion coefficients using the Hall–Morabito method was carried out for film after combined treatment (Fig. 3, *d*) compared to the ion irradiated sample (Fig. 3, *b*), which was taken as the initial state. The estimated lattice diffusivities of Ni in Cu and Cu in Ni (after ion irradiated with an energy of 800 eV and with a duration of 20 minutes) and irradiated and annealed at 450°C for 15 minutes are also summarized in Table 2. According to these data, there is no significant increase in the diffusion coefficient of Cu when using ion pretreatment, while for Ni the diffusivity increases by about 2.3 times. It is worth emphasizing once again that these estimations concern the Ni/Cu interface only and are not applicable to more remote regions of low concentrations, which characterize grain boundary diffusion.

One should consider also other factors that can affect the adhesion for the case of complex treatment. As has been shown recently [20], the increased surface presence of Ar has been detected after the thin film low-energy ion irradiation and thermal treatment. It has been suggested that in this case the implanted Ar atoms may be more strongly bound to metal lattice atoms, as thin films have a less perfect crystal structure than the corresponding bulk metals. Therefore, the relatively low temperature of heat treatment is not enough for complete desorption of im-

planted particles from the near-surface layers, not least due to the growth of the oxide layer on the surface. In this case, the implanted Ar atoms can interfere the movement of dislocations during heat treatment (*i.e.*, to act as Cottrell atmospheres [51]), and thus contribute to the strengthening of the material, which explains the improvement of microtribological characteristics of films after combined exposure. A. Lazauskas *et al.* [6] even suggest that a chemical reaction between Cr and Ar can occur during heating. Embedded Ar atoms can change their traditional inert state and engage into a stronger chemical interaction with the surrounding metal atoms. The ability of heavy noble gases to participate in various chemical transformations does not contradict to the current knowledge on the nature of chemical bonds [49].

Thus, during ion irradiation, there is a competition between the processes of structural defects formation and Ar ions implantation, which oppositely affect the adhesive strength. During the combined treatment, thermal annealing of structural defects occurs, while particular number of the implanted Ar atoms remains in the film. It is also characteristic for such treatment mode that the Ni crystallite size and the roughness are minimal, with reduced presence of carbon impurity atoms in the adhesive bottom layer. The synergistic effect of these factors improves the adhesive strength of the system, whereas neither heat nor ion treatments separately allow to achieve such a positive effect.

5. CONCLUSIONS

It has been demonstrated in present study that the progressive scratch test is an effective technique for characterization of the scratch resistance and adhesion properties of thin metal films. An expedience of applying the preliminary low-energy ion irradiation of the Ni(25 nm)/Cu(25 nm)/Cr(25 nm) thin films prior to thermal treatment has been revealed by means of the enhanced scratch resistance and adhesive strength.

The positive effect of complex ion-heat treatment on the microtribological characteristics is likely associated with the synergistic effect of several factors: reduced number of impurities (especially carbon presence at the Cr/Si interface); decreased crystalline size and surface roughness; Ar atoms implantation at the pre-irradiation stage, which in further become an obstacle to the movement and annealing of dislocations under annealing. However, ion treatment itself does not provide such a clear positive effect, as there is a more fragile nature of the material destruction under conditions of high loads accompanied by the formation of lateral microcracks.

This publication is based on work supported by a grant (#G-202108-68019) from the U.S. Civilian Research & Development Foundation

(CRDF Global). Any opinions, findings and conclusions or recommendations expressed in this material are those of the authors and do not necessarily reflect the views of CRDF Global. This study has been also partially supported by the Project Grant #0121U110283 of the Ministry of Education and Science of Ukraine.

REFERENCES

1. J. M. Martinez-Duart, R. J. Martin-Palma, and F. Aguillo-Rueda, *Nanotekhnologii dlya Mikro- i Optoelektroniki* [Nanotechnologies for Micro- and Optoelectronics] (Moscow: Tehnosfera: 2007) (Russian translation).
2. B. N. Chapman, *J. Vac. Sci. Technol.*, **11**, No. 1: 106 (1974).
3. B. S. Yadav, A. C. Badgujar, and S. R. Dhage, *Solar Energy*, **157**: 507 (2017).
4. K. L. Mittal, *Electrocomponent Sci. Technol.*, **3**: 21 (1976).
5. A. Lassnig, B. Putz, S. Hirn, D. M. Többens, C. Mitterer, and M. J. Cordill, *Materials and Design*, **200**: 109451 (2021).
6. A. Lazauskas, V. Grigaliūnas, A. Guobienė, M. Andrulevičius, and J. Baltrusaitis, *Thin Solid Films*, **520**: 6328 (2012).
7. A. G. Shaucukov, *Prikladnaja Fizika*, No. 5: 16 (2006) (in Russian).
8. H. Javed, B. Merle, E. Preiß, R. Hivet, A. Benedetto, and M. Gökena, *Surf. Coatings Technol.*, **289**: 69 (2016).
9. L. E. Collins, J. G. Perkins, and P. T. Stroud, *Thin Solid Films*, **4**: 4145 (1969).
10. P. T. Stroud, *Thin Solid Films*, **11**: 1 (1972).
11. S. Zuccon, E. Napolitani, E. Tessarolo, P. Zuppella, A. J. Corso, F. Gerlin, M. Nardello, and M. G. Pelizzo, *Opt. Mater. Express*, **5**: 176 (2014).
12. M. A. Vasylyev, B. N. Mordyuk, S. I. Sidorenko, S. M. Voloshko, I. O. Kruhlov, and V. I. Zakiev, *Surf. Coatings Technol.*, **361**: 413 (2019).
13. H. Windischmann, *J. Appl. Phys.*, **62**: 1800 (1987).
14. K. Zhang, M. Wena, G. Cheng, X. Li, Q. N. Meng, J. S. Lian, and W. T. Zheng, *Vacuum*, **99**: 233 (2014).
15. M. O. Vasylyev, S. I. Sidorenko, S. M. Voloshko, and T. Ishikawa, *Usp. Fiz. Met.*, **17**, No. 3: 209 (2016).
16. I. O. Kruhlov, I. A. Vladymyrskyi, O. Dubikovskyi, S. I. Sidorenko, T. Ebisu, K. Kato, O. Sakata, T. Ishikawa, Y. Iguchi, G. A. Langer, Z. Erdélyi, and S. M. Voloshko, *Mater. Research Express*, **6**: 126431 (2019).
17. G. J. Klingenmaier and M. Dobrash, *Adhesion Measurement of Thin Films, Thick Films and Bulk Coatings* (Ed. K. L. Mittal) (Philadelphia: ASTM: 1978), p. 369.
18. E. Darque-Ceretti and E. Felder, *Adhesion et Adherence. Sciences et Techniques de L'ingenieur* (Paris: CNRS Editions: 2003), p. 246.
19. A. A. Volinsky, N. R. Moody, and W. W. Gerberich, *Acta Mater.*, **50**: 441 (2002).
20. I. Kruhlov, A. Orlov, V. Zakiev, I. Zakiev, S. Prikhodko, and S. Voloshko, *TMS 2022 151st Annual Meeting Exhibition Supplemental Proceedings (February 27–March 3, 2022)* (Anaheim: 2022), p. 431.
21. S. V. V. N. Siva Rao, T. Bhavani, S. K. Ghosh, J. D. Barma, and R. K. B. Meitei, *Materials Today: Proceedings*, **47**, Part 11: 3400 (2021).
22. M. Storchak, I. Zakiev, V. Zakiev, and A. Manokhin, *Measurement*, **191**: 110745 (2022).
23. O. Borrero-Lypez, M. Hoffman, A. Bendavid, and P. J. Martin, *Thin Solid*

Films, **518**: 4911 (2010).
24. E. Broitman, *Tribol. Lett.*, **65**: 23 (2017).
25. S. R. Ignatovich, I. M. Zakiev, D. I. Borisov, and V. I. Zakiev, *Strength Mater.*, **38**: 428 (2006).
26. S. J. Bull, *Surf. Coat. Technol.*, **50**, Iss. 1: 25 (1991).
27. J. Malzbender, J. M. J. den Toonder, A. R. Balkenende, and G. de With, *Mater. Sci. Eng. R*, **36**, Iss. 2–3: 47 (2002).
28. V. Hutsaylyuk, M. Student, V. Posuvailo, O. Student, V. Hvozdets'kyi, P. Maruschak, and V. Zakiev, *J. Mater. Res. Technol.*, **14**: 1682 (2021).
29. V. A. Mechnik, N. A. Bondarenko, V. M. Kolodnitskyi, V. I. Zakiev, I. M. Zakiev, E. S. Gevorkyan, N. O. Kuzin, O. S. Yakushenko, and I. V. Semak, *J. Superhard Mater.*, **41**, No. 1: 43 (2021).
30. O. B. Zgalat-Lozynskyy, O. O. Matviichuk, O. I. Tolochyn, O. V. Ievdokymova, N. O. Zgalat-Lozynska, and V. I. Zakiev, *Powder Metall. Metal Ceramics*, **59**: 515 (2021).
31. X. Wang, P. Xu, R. Han, J. Ren, L. Li, N. Han, F. Xing, and J. Zhu, *Nanotechnol. Rev.*, **8**, No. 1: 628 (2019).
32. J. Li and W. Beres, *Canadian Metallurgical Quarterly*, **46**, Iss. 2: 155 (2007).
33. M. S. Kabir, P. Munroe, Z. Zhou, and Z. Xie, *Wear*, **380–381**: 163 (2017).
34. S. J. Bull and E. G. Berasetegui, *Tribology International*, **39**, Iss. 2: 99 (2006).
35. N. Schwarzer, Q.-H. Duong, N. Bierwisch, G. Favaro, M. Fuchs, P. Kempe, B. Widrig, and J. Ramm, *Surf. Coat. Technol.*, **206**: Iss. 6: 1327 (2011).
36. K. Khojier, H. Savaloni, Z. Ashkabusi, and N. Z. Dehnavi, *Applied Surf. Sci.*, **284**: 489 (2013).
37. I. Zakiev, M. Storchak, G. A. Gogotsi, V. Zakiev, and Y. Kokoieva, *Ceramics Int.*, **47**, Iss. 21: 29638 (2021).
38. M. Zawischa, M. M. A. B. M. Supian, S. Makowski, F. Schaller, and V. Weihnacht, *Surf. Coat. Technol.*, **415**: 127118 (2021).
39. M. Laugier, *Thin Solid Films*, **76**, Iss. 3: 289 (1981).
40. Woei-Shyan Lee and Te-Yu Liu, *Nanotechnology*, **18**: 335701 (2007).
41. A. M. Kovalchenko, S. Goel, I. M. Zakiev, E. A. Pashchenko, and R. Al-Sayeghe, *J. Mater. Res. Technol.*, **8**, Iss. 1: 703 (2019).
42. N. Tayebi and A. A. Polycarpou, *Microsyst. Technol.*, **12**: 854 (2006).
43. B. Stegemann, H. Backhaus, H. Kloss, and E. Santner, *Modern Research and Educational Topics in Microscopy* (Eds. A. Méndez-Vilas and J. Díaz) (Formatex, Spain: 2007), vol. 1, p. 824.
44. W. M. Dawson and F. R. Sale, *Metall. Trans. A*, **8**: 15 (1977).
45. P. M. Hall and J. M. Morabito, *Surf. Sci.*, **54**: 79 (1976).
46. S. Lian, A. Fourie, J. Wang, H. C. Swart, and J. J. Terblans, *Vacuum*, **202**: 111206 (2022).
47. X. Cen, A. M. Thron, and K. van Benthem, *Acta Mater.*, **140**: 149 (2017).
48. H. Ryssel and L. Ruge, *Ion Implantation* (Chichester: John Wiley Sons Ltd., Hoboken: 1986).
49. M. O. Vasylyev, S. I. Sidorenko, I. O. Kruhlov, and D. I. Trubchaninova, *Metallofiz. Noveishie Tekhnol.*, **42**, No. 5: 621 (2020) (in Ukrainian).
50. Y. G. Chabak, V. I. Fedun, K. Shimizu, V. G. Efremenko, and V. I. Zurnadzhy, *Problems of Atomic Science and Technology*, No. 4 (102): 100 (2016).
51. O. Waseda, R. GA Veiga, J. Morthomas, P. Chantrenne, C. S. Becquart, F. Ribeiro, A. Jelea, H. Goldstein, and M. Perez, *Scripta Mater.*, **129**: 16 (2017).